This article has been accepted for inclusion in a future issue of this journal. Content is final as presented, with the exception of pagination.

Compensation of Geometric, Backlash, and Thermal Drift Errors Using a Universal Industrial Robot Model

Pirmin Sigron, Ivo Aschwanden, and Markus Bambach

***Abstract*— In order to facilitate the use of articulated robots for complex industrial applications, methods to improve the absolute positioning accuracy are needed. This work introduces a robot-independent calibration procedure that allows to compensate for geometric and backlash errors as well as for thermal drift. To this end, a unifying robot model is introduced based on the product of exponentials formula that complies with the requirements of the calibration process. The model is able to represent any kind of serial kinematic chain, which guarantees universal applicability. The full parameter identification is performed simultaneously based on a single data set containing all modeled effects. The individual modeling approaches have been verified experimentally using two different industrial robots. The positioning accuracy could be improved to industrial standards within the selected workspace. More precisely, the average position error was reduced from 3.39mm to 0.13mm for a KUKA KR-16 robot and from 0.36mm to 0.12mm for a KUKA KR-30 within all operating conditions. The generalizing property of the thermal expansion model was assessed by compensating the thermal drift for an unseen and fundamentally different thermal excitation of the robot structure, limiting the thermally induced positioning error to 0.1mm.**

***Note to Practitioners*—This paper was motivated by the fact that modern industrial robots are known to be able to execute the same movement repeatedly with high precision but are unable to visit an arbitrary sequence of commanded positions with high accuracy. In practice, this means that each pose of a given process must be taught to the robot by moving it to the target position and storing the robot's posture. To overcome this limitation, this work introduces a robot model that is able to express the geometric properties of the robot, as well as the joint backlash and the thermal expansion of the robot links. The model parameters must be evaluated based on a measurement sequence of 300-400 robot poses during the heating up of the robot structure. Therefore, depending on the size of the robot, the calibration procedure takes one to four hours. To use the thermal expansion correction, real-time measurements based on four low-cost temperature sensors are used. Since the modeled robot characteristics only change due to long-term wear, there is no need to repeat the calibration procedure frequently. The introduced calibration method allows to move the robot to arbitrary positions or along arbitrary trajectories within the employed workspace, with a positioning error of less than 0.2mm. This facilitates non-repetitive pick and place, assembly, or additive manufacturing tasks.**

Manuscript received 7 July 2023; revised 16 October 2023; accepted 23 October 2023. This article was recommended for publication by Associate Editor G. Palli and Editor P. Rocco upon evaluation of the reviewers' comments. *(Corresponding author: Pirmin Sigron.)*

The authors are with the Advanced Manufacturing Laboratory, ETH Zürich, 8005 Zürich, Switzerland (e-mail: sigronp@ethz.ch; aschwanden@inspire.ethz.ch).

Digital Object Identifier 10.1109/TASE.2023.3328835

***Index Terms*— Robot calibration, product of exponentials, thermal drift compensation, backlash compensation.**

I. Introduction

With the continuing automation of wide parts of the industry, the demand for highly accurate industrial robots is increasing. Due to their ability to repeatedly follow the same trajectory or to revisit a pose with high precision (high repeatability), they are widely used for repetitive tasks like welding or spray painting. To be able to deploy industrial robots for more complex tasks, their absolute positioning accuracy must be increased. To date, there are two main concepts for improving accuracy: (i) static compensation or calibration, where the robot's behavior is studied before operation and a robot model is then used to compensate for different types of errors [1], [2], [3], and (ii) dynamic or online compensation, where real-time measurement data is used to directly correct for unwanted deviations [4], [5], [6]. Further, combinations of the two concepts have been proposed [7]. Dynamic compensation is able to concurrently deal with diverse types of disturbances and is therefore particularly interesting for high-load applications or tasks with varying external forces. However, it comes with a high system complexity, affecting reliability in harsh environments, and generally requires expensive measurement systems that must be available during operation. On the other hand, the performance of static compensation approaches generally decreases for an increasing workspace size, and it is difficult to guarantee high accuracy for different working conditions [8], [9]. Nevertheless, static compensation approaches are of high relevance for applications with low loads that lead to small structural deformations, like pick-and-place tasks, assembly, additive manufacturing, drilling, 3D-measuring, or laser cutting. To facilitate the deployment of industrial robots for non-repetitive and high-accuracy applications, this work aims to develop a generally applicable error compensation method that avoids online position measurements during operation.

The most important effects reducing the robot's accuracy during operation are geometric errors, thermal deformation, compliance of the robot structure, and joint transmission inaccuracies, which in turn include backlash, joint compliance, and harmonic drive errors. Multiple effects have to be considered simultaneously to improve the positioning accuracy to meet industrial standards. Since this renders the modeling of industrial robots more complex, some efforts have been made to use

© 2023 The Authors. This work is licensed under a Creative Commons Attribution-NonCommercial-NoDerivatives 4.0 License.
For more information, see https://creativecommons.org/licenses/by-nc-nd/4.0/

This article has been accepted for inclusion in a future issue of this journal. Content is final as presented, with the exception of pagination.

parametric models such as neural networks [10], [11], [12], [13] or combinations of geometric and parametric approaches [9]. While these models succeed in capturing highly complex behavior, they do not generalize and thus require a large amount of measurements to cover the entire workspace and different operation modes. For the practical application of any compensation technique, we deem it important to limit the number of measurements to a feasible amount. Therefore, a simpler model with a minimal number of parameters that generalizes to unseen data is needed.

For the calibration procedure to be universally applicable and the model parameters to be identifiable, the robot model must meet the following key requirements:

- **Generalizing** - Capability to represent all kinematic chains independently of their structural configuration. This allows to apply the same model to different serial industrial robots without changing the model parameters [1].
- **Continuous** - The kinematic map from the model parameters to the end-effector pose is at least free from singularities (for the parameter identification, differentiability is favorable) within the entire robot parameter space, meaning that small changes in the robotic structure always lead to small changes in the model parameters [1], [14].
- **Minimal** - The number of independent kinematic parameters corresponds to the minimal number of parameters necessary to describe the full state of the kinematic chain (6 parameters for an unconstrained body, 4 for a revolute joint and 2 for a prismatic joint [1], [15]).

This work presents an error compensation method for industrial robots that avoids case-specific modeling. It combines the main disturbing effects that reduce the robot accuracy for static and low load applications in a single model. Namely, these are geometric errors, thermal deformation, and backlash. The presented approach allows to simultaneously identify all model parameters in a single optimization and on a single data set, which facilitates the application of the approach in practice. Besides complying with the key requirements for a calibration model, the compensation technique is valid within the full predefined workspace and for different thermal excitations.

A. Contributions

The main contributions of this work are:

- Reformulation of the product of exponentials formula in an explicit way (the parameters of the standard POE model do not correspond to explicit geometrical features of the robot), allowing to merge a thermal expansion model with kinematic calibration and backlash compensation. This unifying model can be applied to any open serial kinematic structure, omitting case-specific modeling, and complies with the requirements of a calibration model.
- Simultaneous identification of all model parameters based on a single data set, comprising all disturbances to be identified. Thus, facilitating the application in practice and ensuring optimality of the identified parameters.
- Detailed validation of thermal drift compensation, using two substantially different thermal excitations for training and validation, to assess its generalizing property.
- Verification of the full compensation method on two different industrial robots, proving that the method is transferable without case-specific adaptations.
- Analysis of the influence of the size of the workspace (calibration space) on the calibration performance.

B. Related Work

This section first briefly introduces the state of the art of robot models used for calibration purposes, before focusing on existing works that compensate for multiple disturbing effects simultaneously.

To date, the most widely used description technique for the kinematics of industrial robots is the Denavit-Hartenberg (D-H) model. It offers an intuitive way of modeling kinematic chains, but during the parameter identification, it suffers from singularities for consecutive joints with parallel rotation axes [1]. This issue can be solved by introducing a modification to the D-H model [16], which in turn leads to a robot model that depends on the structure of the kinematic chain. Further variations of the D-H convention, like the Stone model [17] and the complete and parametrically continuous (CPC) model [18], were suggested. In these, two additional parameters are introduced in order to solve the singularity issues, resulting in redundant parameters. Another approach to avoid singularities in the robot model description is the product of exponentials (POE) formula [14]. It makes use of the screw theory and can, by design, represent any kind of open kinematic chain, since it can deal with revolute, prismatic, and even helical joints [15], [19]. Its math is based on Lie group theory and gives rise to efficient recursive algorithms to calculate forward and inverse kinematics [20], but lacks an intuitive and concise geometric interpretation of the robot [15].

A majority of the work related to calibration presented so far focuses on identifying a single aspect of the robotic system and its compensation. Nonetheless, some studies were conducted where kinematic error compensation was combined with joint compliance correction or thermal drift compensation. In the following, a survey of the most relevant publications related to the present work is provided.

1) Kinematic Calibration and Joint Error Compensation: One of the first works to combine a kinematic model with joint compliance estimation was proposed by *Nubiola* et al. [21]. They made use of the D-H convention and additionally identified higher-order transmission errors in joint 6. They used measurements within the entire joint space to identify the model parameters and validated the robot model in a cube with a side length of $0.7m$. A similar approach was proposed by Deng et al. [22], which combined a kinematic and joint compliance model. They used a two-step method based on sequential floating forward selection to find the optimal set of robot configurations for parameter identification. They experimentally validated their method on a KUKA KR-160 along certain predefined trajectories. Cho et al. [23] adopted the POE model and augmented it with a joint compliance

This article has been accepted for inclusion in a future issue of this journal. Content is final as presented, with the exception of pagination.

correction. They applied the circular point analysis to identify the model parameters and validated the method experimentally. Luo et al. [24] presented a combined model, considering the geometric errors and joint compliance based on the POE formula. Similarly, Song et al. [25] developed a model combining geometric and arbitrary deformation errors of the structure. The results of all these approaches show that the combination of kinematic and joint error compensation can reduce the positioning error by a significant amount. However, none of these methods consider changing temperature fields and the resulting thermal drift.

2) Kinematic Calibration and Thermal Drift Compensation: Few works dealing with real-time thermal drift compensation for industrial robots have been presented so far. Li et al. [26] proposed an online compensation method where a calibration procedure is executed as soon as the mean positional error of 4 reference positions exceeds a certain value. For the compensation, position measurements of 4 different poses are used to slightly adjust the kinematic parameters. A similar online compensation method was proposed by Yin et al. [27]. They used a laser scanner to measure reference spheres to collect data that is used to correct the robot model parameters. For both methods, it is necessary to interrupt the robot operation to keep track of the thermal drift, and a laser measuring device must be accessible during operation. This we deem impractical for most applications and therefore aim to avoid with our method. Vocetka et al. [28] suggested a method to compensate for thermal drift at specific robot configurations to ensure high repeatability during operation. The method uses data from temperature sensors mounted at the joints and directly learns the thermal drift of the tool center point (TCP) in each direction, reducing the positioning repeatability at the predefined pose. However, with this method, the thermal drift can only be compensated at a few distinct poses and does not generalize to the full workspace.

3) Kinematic Calibration, Joint Error and Thermal Drift Compensation: The first to introduce a procedure to simultaneously correct kinematic errors, joint compliance, and thermal drift were Gong et al. [29]. They presented a model-based compensation approach where the calibration procedure is split into two parts. In the first step, the kinematics and joint compliance are identified at room temperature, assuming constant temperature of the robot structure. The calibrated models are then used to empirically find the temperature-dependent changes of the kinematic model parameters based on temperature measurements at several links. For validation, they uniformly increased the joint speed on all joints from 50% to 65% of maximum speed. However, this does not represent a substantially different thermal excitation, such that only limited conclusions can be made about how well the method generalizes. Furthermore, they encountered the previously mentioned issues with singularities when applying the D-H convention for modeling, and introduced an additional case-specific parameter to overcome them.

Another approach that combines kinematic and backlash errors with thermal drift compensation and is based on the modified D-H model was proposed by Le Reun et al. [30]. Due to the geometric parameters being needed to identify the thermal ones, the parameter identification is performed separately for the geometric and thermal models. The backlash is compensated only for the first joint because the examined trajectory does not introduce further backlash issues. Since this method is designed to improve the accuracy for repetitive tasks, the proposed model was not validated in the full workspace or for a different thermal excitation. The so far presented works proved that the combination of kinematic calibration with joint error and thermal drift compensation can improve positioning accuracy. Nonetheless, a generally applicable method for combining the three models (without the need for case-specific modeling) and identifying the model parameters simultaneously on a single data set (to ensure optimality) has yet to be found. Furthermore, it is left to be shown that the thermal drift compensation can be applied to different, previously unknown temperature fields.

II. Robot Model

A. Robot Kinematics

The following section provides a basic introduction to the POE formula and introduces the nomenclature for later use. For a detailed mathematical description, the reader is referred to [14]. The forward kinematics expressed using the POE formula take the form

$$\mathbf{T}_{b,ee}(\mathbf{q}) = \exp(\bar{\boldsymbol{\xi}}_1 q_1)\exp(\bar{\boldsymbol{\xi}}_2 q_2)\cdots\exp(\bar{\boldsymbol{\xi}}_n q_n)\mathbf{T}_{b,ee}(\mathbf{0}) \quad (1)$$

where $\mathbf{T}_{b,ee}(\mathbf{q})$ denotes the homogeneous transformation matrix of the end-effector (ee) represented in the base (b) coordinate frame, depending on the vector of joint angles $\mathbf{q}$. The matrix form of the twist $\bar{\boldsymbol{\xi}}_i$ belongs to the Lie algebra $se(3)$ and is given by

$$\bar{\boldsymbol{\xi}}_i = \begin{bmatrix} \bar{\boldsymbol{\omega}}_i & \mathbf{v}_i \\ 0 & 0 \end{bmatrix}, \quad (2)$$

where $\mathbf{v}_i \in \mathbb{R}^3$ can be interpreted as the instantaneous velocity of the base frame given an angular joint velocity of $\dot{q}_i = 1\frac{rad}{s}$ [31], and $\bar{\boldsymbol{\omega}}_i$ is the skew-symmetric matrix of the angular velocity vector $\boldsymbol{\omega}_i$.[1] Furthermore, $\mathbf{v}_i$ can be computed as

$$\mathbf{v}_i = \mathbf{p}_i \times \boldsymbol{\omega}_i + h_i \boldsymbol{\omega}_i, \quad (3)$$

where $\mathbf{p}_i$ is an arbitrary point on the rotation axis of the joint i represented in the base coordinate frame, and h_i represents the ratio between the translation and the rotation, frequently referred to as pitch. The twist in vector form is given by

$$\boldsymbol{\xi}_i = \begin{bmatrix} \boldsymbol{\omega}_i \\ \mathbf{v}_i \end{bmatrix}. \quad (4)$$

Although the POE formula introduces six parameters for each joint, no redundancy is introduced. For a revolute joint, for instance, the angular velocity vector $\boldsymbol{\omega}$ is constrained to have unit length and be perpendicular to $\mathbf{v}$, which reduces the number of independent kinematic parameters to four.

[1] For a purely revolute joint $\boldsymbol{\omega}_i$ corresponds to the joint rotation axis.

This article has been accepted for inclusion in a future issue of this journal. Content is final as presented, with the exception of pagination.

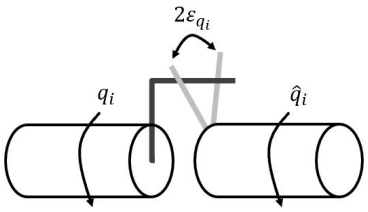

Fig. 1. Illustration of joint backlash, with ε_i denoting the amount of backlash present in joint i.

B. Backlash

An important source of non-linearity in harmonic drives, leading to joint positioning errors of around 0.01°, is backlash [32], [33]. A simple method to capture the most relevant effects is to only consider the joint approach direction [34]. Figure 1 illustrates how the dead zone of the backlash, which leads to the misalignment of the joint, is modeled. The corresponding formula that describes the corrected joint state $\hat{q}_i$ is given by

$$\hat{q}_i = q_i - \bar{q}_i \varepsilon_i. \tag{5}$$

Here, q_i is the nominal joint state of joint i, ε_i denotes the amount of backlash present and $\bar{q}_i$ stands for the joint approach direction, defined as

$$\bar{q} = \begin{cases} 1, & \text{for positive rotation,} \\ -1, & \text{for negative rotation.} \end{cases} \tag{6}$$

C. Thermal Deformation

Due to the complex and operation-specific temperature distribution over the robot (illustrated in figure 2), exact modeling of the thermal expansion of the robot structure is difficult. One of the limiting factors is the availability of temperature data at a reasonable cost. When aiming at gathering information about the exact temperature distribution over the entire robot structure, a large number of temperature sensors or a thermal camera have to be installed, leading to unfeasible system costs. Since the gradients of the temperature distribution in the links are small (as shown in figure 2), a finite number of temperature sensors suffices to capture the thermal effects. Previous work showed that the thermally induced change of the link geometry constitutes the predominant thermal effect reducing the robot accuracy [29], [30]. In this work, the link elongation along the main dimension is modeled, since it is expected to play a substantial role. A single temperature sensor per link is used, and the model assumes uniform temperature distribution over each link. It follows the linear thermal expansion formula, assuming constant linear expansion coefficients, which is reasonable for the temperature variations considered in this work as supported by [35]. The corresponding formula describing the temperature-dependent link length is given by

$$l_i(\tau_i) = l_{i,0} \cdot (1 + \alpha_i \cdot (\tau_i - \tau_0)), \tag{7}$$

with l_i being the length of link i, $l_{i,0}$ the nominal link length, α_i denoting the linear thermal expansion coefficient of link i, and τ_i the measured temperature of the link. Since the nominal

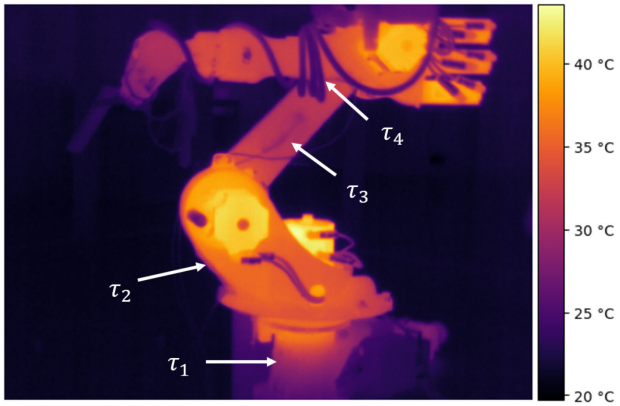

Fig. 2. Temperature distribution of the KUKA KR-16 after 4 hours of operation. The white arrows highlight the locations of the temperature sensors (τ_1 to τ_4) used in the experiments.

link length $l_{i,0}$ and the thermal expansion coefficient α_i are identified simultaneously, the reference temperature τ_0 can be chosen arbitrarily without loss of generality and was set to $20°C$ in the present work.

D. Combined Robot Model

To be able to compensate for the geometric and backlash errors as well as for the thermal drift simultaneously, a description was developed that combines the aforementioned models. When applying the traditional POE formulation, the corresponding twists $\boldsymbol{\xi}_i$ for all joints of the robot are defined using the joint angular velocity vector $\boldsymbol{\omega}_i$, the pitch h_i, and a point on the rotation axis represented in the base coordinate frame $\mathbf{p}_i$. Since this formulation does not provide an explicit representation of the robot geometry (link length), the temperature-dependent relative joint position vector $\mathbf{d}_i(\tau_i)$ is introduced. This vector describes the position of joint i relative to joint $i-1$ in robot zero position ($\mathbf{q} = \vec{\mathbf{0}}$), expressed in base frame coordinates. As the linear thermal expansion relation introduced in 7 suggests, the temperature dependence of the joint positions (link lengths) can be expressed as a scaling of the nominal relative joint positions $\mathbf{d}_{i,0}$, yielding

$$\mathbf{d}_i(\tau_i) = \mathbf{d}_{i,0} \cdot (1 + \alpha_i \cdot (\tau_i - \tau_0)). \tag{8}$$

The corrected relative joint positions can then be used to find the temperature-dependent joint position $\mathbf{p}_i(\tau_i)$ expressed in base frame coordinates, leading to

$$\mathbf{p}_i(\tau_i) = \sum_{j=1}^{i} \mathbf{d}_i(\tau_i). \tag{9}$$

Now, the twist corresponding to joint i can be determined using

$$\boldsymbol{\xi}_i(\tau_i) = \begin{bmatrix} \boldsymbol{\omega}_i \\ \mathbf{p}_i(\tau_i) \times \boldsymbol{\omega}_i + h_i \boldsymbol{\omega}_i \end{bmatrix}. \tag{10}$$

Analogously to the joint positions, the end-effector position in robot zero-position is determined using the corrected relative

This article has been accepted for inclusion in a future issue of this journal. Content is final as presented, with the exception of pagination.

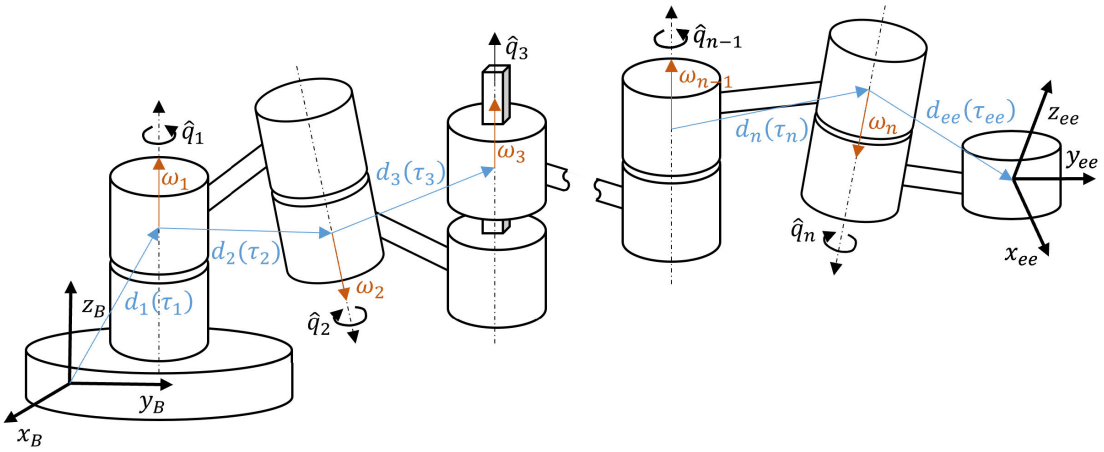

Fig. 3. Illustration of universally applicable robot model combining kinematics, backlash and thermal expansion.

joint positions and the temperature-dependent relative end-effector position $\mathbf{d}_{ee}(\tau_i)$:

$$\mathbf{p}_{ee}(\tau_i) = \mathbf{d}_{ee}(\tau_{ee}) + \sum_{j=1}^{n} \mathbf{d}_i(\tau_i). \tag{11}$$

Overall, each joint of the articulated kinematic chain is parametrized by a joint angular velocity vector $\boldsymbol{\omega}$, the nominal relative joint position $\mathbf{d}_{i,0}$, a thermal expansion coefficient α_i, the pitch h_i and the backlash amount ε. Furthermore, the homogeneous transformation matrix $\mathbf{T}_{b,ee}(\mathbf{0})$ describing the end-effector pose in zero-position is required. It is parametrized by the nominal relative end-effector position $\mathbf{d}_{ee,0}$, the thermal expansion coefficient α_{ee} and three parameters defining the orientation of the end-effector with respect to the base coordinate frame. The combined model is obtained by inserting the corrected joint states $\hat{q}_i$, the temperature-dependent joint twists $\boldsymbol{\xi}_i(\tau_i)$ and the homogeneous transformation matrix $\mathbf{T}_{b,ee}(\mathbf{0})$ into (1). Figure 3 illustrates the modeling approach for an arbitrary open kinematic chain.

It is left to check that the introduced model complies with the requirements of a universally applicable calibration model. Namely, it must be (i) generalizing, (ii) continuous, and (iii) minimal.

- (i) Since the POE formula is able to represent any kind of kinematic chain, the generalizing property is given.
- (ii) *Park O.* et al. and *He R.* et al. proved that the POE formula constitutes a differentiable map [14], [36]. As continuity is required for a function to be differentiable, this implies continuity of the POE formula. Furthermore, the backlash and thermal expansion models represent continuous maps of their respective parameters. Based on the following three characteristics of continuous functions, it can be shown that, indeed, the combined model is a continuous map: (1) the sum of two continuous functions is continuous, (2) the product of two continuous functions is continuous (product rule) and (3) the composition of two continuous functions is continuous (chain rule).
- (iii) Neither the backlash model nor the thermal expansion model introduces redundant parameters to the POE formula, leading to a minimal representation.

III. Parameter Identification

Generally speaking, parameter identification aims at finding a set of model parameters that minimize the difference between the output of the robot model and real-world measurement data. Therefore, not only the choice of the model but also the quality and information content of the measurement data are decisive for the success of a calibration. Additionally, the parameter identification strategy needs to be chosen, including a cost function and an optimization algorithm. In the following, the parameter identification carried out within the present work is described in detail.

A. Data Capturing Strategy

In the following, the three most important aspects related to the data capturing strategy are discussed.

First of all, the type, number, and quality of the measurements affect the measurement strategy. For kinematic calibration purposes, most often position or full-pose measurement data is used, obtained through laser tracking or photogrammetric sensing. Since full-pose measurement data contains more information, the number of necessary measurement points can be reduced compared to pure position measuring techniques. Nevertheless, since the measurement process is subject to stochastic uncertainties, a larger amount of measurement data improves the result of the identification process.

Another important component of the data capturing strategy is the choice of workspace. While a large spread of measured poses is favorable for accurate identification of the model parameters and leads to a better generalization, a larger workspace typically results in lower accuracy since additional nonlinearities caused by self-compliance can arise. Generally, the calibration should be performed within the region of the working space with the greatest anticipated use and the smallest volume necessary for the application. Although ISO 9283-1998 [37] suggests a cubic shape to specify the operating area, this definition is hardly used in literature since cylindrical

This article has been accepted for inclusion in a future issue of this journal. Content is final as presented, with the exception of pagination.

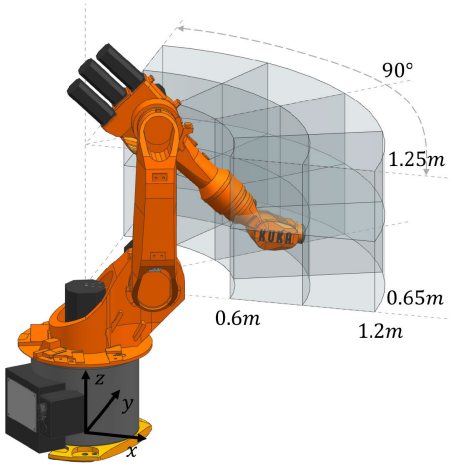

Fig. 4. Illustration of workspace.

TABLE I
MOVING RANGE DURING THERMAL EXCITATION

Joint	1	2	3	4	5	6
range [°]	58	63	70	70	90	90

or spherical operating volumes are better choices for utilizing the reach of industrial robots, resulting in larger workspaces compared to the ISO-cube. Figure 4 illustrates the workspace used in this work. The size can be proportionally adjusted according to the robot range. It should be noted that in this text, the term workspace is used to refer to the end-effector position space.

For the calibration to be successful, it is crucial to adapt the pose sampling strategy such that the effects to be identified are represented within the measured data set. For instance, to identify the thermal characteristics, the thermal excitation of the robot structure must be large enough. The heat emitted by the motors and the joints correlates with the speed and range of the movement on the respective axis (energy introduced by the motors). This can be used to induce different thermal excitations to the system, comparable to different industrial applications. In this work, two different heating procedures are used where either all or only three joints are simultaneously moved within a predefined range given in table I. The joint ranges are chosen, such that each motor heats up to approximately the same temperature. Furthermore, for the calibration to be representative of industrial applications, the measured poses are randomly sampled with uniform distribution within the chosen workspace, and the orientation is rotated towards the tracking device, with a permitted deviation of 15°, to ensure visibility of the tracking target. It should be noted that this procedure limits the domain of inspected orientations. The random sampling of the measurement poses ensures arbitrary approach direction on joint state level and therefore allows to identify the backlash in the respective joints.

B. Objective Function

The objective function is defined as the average of residuals. It combines the position and orientation deviation from the modeled forward kinematics to the measured data. The cost is given by

$$F(\mathbf{x}) = \frac{1}{n}\sum_{i=1}^{n}(\left\|\mathbf{p}_{ee}(\mathbf{x},\mathbf{q}_i) - \mathbf{p}_{m_i}\right\| + w \cdot \Delta\theta(\mathbf{x},\mathbf{q}_i)), \quad (12)$$

where $\|\cdot\|$ denotes the euclidean norm, $\mathbf{x}$ is a vector containing the model parameters, $\mathbf{p}_{ee}(\mathbf{x},\mathbf{q}_i)$ and $\mathbf{p}_{m_i}$ denote the estimated and measured position of the end-effector at the i-th pose, w is a weighting parameter used to tune the weight of the orientation error and $\Delta\theta(\mathbf{x},\mathbf{q}_i)$ describes the orientation error. The latter can be understood as the magnitude of the shortest possible rotation between the estimated and measured end-effector orientation. It can be computed according to

$$\Delta\boldsymbol{R}(\mathbf{x},\mathbf{q_i}) = \mathbf{R}_{ee}(\mathbf{x},\mathbf{q_i})^T \cdot \mathbf{R}_{ee,m_i} = \begin{bmatrix} r_{11} & r_{12} & r_{13} \\ r_{21} & r_{22} & r_{23} \\ r_{31} & r_{32} & r_{33} \end{bmatrix}, \quad (13)$$

where the rotation matrices $\mathbf{R}_{ee}(\mathbf{x},\mathbf{q_i})$ and $\mathbf{R}_{ee,m_i}$ represent the orientation of the estimated and measured pose respectively. The orientation error is then given by

$$\Delta\theta(\mathbf{x},\mathbf{q}_i) = \arccos\left(\frac{r_{11}+r_{22}+r_{33}-1}{2}\right). \quad (14)$$

The weighting factor w is determined based on the relative importance of the orientation compared to the position in a specific application. In this work, the weighting parameter was set such that the cost of 0.5° orientation error is roughly the same as the cost of $1mm$ position error. Since $\mathbf{p}_{ee}(\mathbf{x},\mathbf{q}_i)$ and $\mathbf{p}_{m_i}$ are given in m and $\Delta\theta(\mathbf{x},\mathbf{q}_i)$ is given in rad, the weighting factor is determined by

$$w = 0.1m \approx 0.115m = \frac{0.001m \cdot 180°}{0.5° \cdot \pi}. \quad (15)$$

Intuitively, the weighting factor can be understood as the length of a tool which, when mounted at the end-effector, leads to $1mm$ misalignment for 0.5° orientation error.

C. Model Parameter Identification

A variety of nonlinear algorithms are readily available today. Therefore, it is unnecessary to develop a specific identification algorithm for the given problem. After testing a variety of optimization algorithms, sequential least squares programming (SLSQP) was chosen for the present work because of its favorable convergence behavior. In order to avoid constrained optimization and ensure convergence of the optimization algorithm, the model parameters were reparameterized and scaled before optimization.

1) Reparameterization of Model Parameters: As described in section II-D, the introduced robot model is able to represent arbitrary types of joints. To account for the fact, that the industrial robots used within this work only include revolute joints, the number of independent model parameters needs to be reduced. One way of doing so is to impose constraints on the kinematic robot parameters. Although there exist a number of sophisticated algorithms for constrained optimization, they do not guarantee to stay inside the constraints during optimization, which for the given problem causes numerical

This article has been accepted for inclusion in a future issue of this journal. Content is final as presented, with the exception of pagination.

TABLE II
PROPERTIES OF THE DEPLOYED INDUSTRIAL ROBOTS

Type	KR-16	KR-30
Year of manufacture	2007	2010
Maximum reach	$1.61m$	$2.03m$
Approx. weight	$235kg$	$665kg$
Rated payload	$16kg$	$30kg$
Rated repeatability (ISO 9283)	$\pm 0.05mm$	$\pm 0.15mm$

problems. Moreover, constrained optimization is generally computationally expensive, leading to increased computing time. Besides setting the joint pitch h to zero, a reformulation of the joint angular velocity vector $\boldsymbol{\omega}$ is introduced for the subsequent parameter identification. Since for revolute joints $\boldsymbol{\omega}$ is restricted to have unit length, an intuitive way of parametrizing an arbitrary direction without introducing discontinuities is to think of it as a unit vector rotated around two perpendicular axes. For instance, by using intrinsic Euler rotations about the z- and y'-axis, a unit vector pointing in x-direction can be rotated to point to an arbitrary direction. Mathematically, this reads

$$\boldsymbol{\omega} = \mathbf{R}_{zy'x''}(\phi, \theta, 0) \cdot \mathbf{e}_x, \tag{16}$$

where ϕ and θ denote the rotation angles about the z- and y'-axis and $\mathbf{e}_x$ refers to the unit vector in x-direction.

2) Parameter Scaling: Recent research showed that the combination of various robot characteristics in a single model can lead to an ill-conditioned optimization problem [38], which can cause bad or no convergence even when applying sophisticated optimization algorithms. This issue was tackled by applying appropriate scaling to the optimization parameters, following the procedure introduced in [39]. The scaling aims at obtaining optimization parameters of similar magnitude and of unity order in the region of interest.

IV. EXPERIMENTAL SETUP

A. Industrial Robots

To validate the generalizing property of the system identification procedure, the calibration was carried out using two different industrial robots, namely a KUKA KR-16-2 (KR-16) and a KUKA KR-30-3 (KR-30). They represent the low and medium payload categories of industrial robots, which are most often used for high-accuracy applications like assembly, measuring, welding, or laser cutting (figure 5 shows the experimental setup with the KR-30). While the KR-30 was refurbished recently, the KR-16 has been deployed in the automotive industry and in research for several years and is expected to suffer from noticeable performance loss due to wear. Table II provides an overview of the most important properties of the robots used in this work. According to ISO 9283-1998, the position repeatability is defined as

$$RP_P = \pm(\bar{P} + 3\sigma_P), \tag{17}$$

where $\bar{P}$ denotes the mean position error and σ_{P_i} means the standard deviation of the position error.

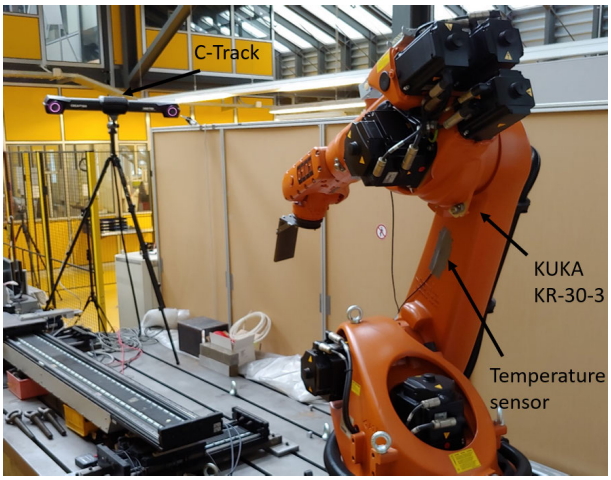

Fig. 5. Experimental setup with the KUKA KR-30.

B. Photogrammetric Sensor

For the pose measurements, a Creaform C-Track was used, which is a photogrammetric sensor that allows for highly accurate full-pose measurements. It is able to track reflectors within a volume of $16.6m^3$ with a rated repeatability of $0.02mm$ and a volumetric accuracy of $0.1mm$ [40]. It allows a measurement rate of $80Hz$.

C. Temperature Sensors

In accordance with the previously introduced model, a single digital temperature sensor was mounted onto each link. For the uniform temperature assumption to work best, the temperature sensors were attached approximately halfway between consecutive joints, using thermal paste to ensure a proper heat transfer between the robot structure and the temperature sensors. The digital temperature sensors attached to the robot are of type DS18B20+ and support a temperature range of -55 to $125°C$ with an accuracy of $\pm 0.5°C$ and a resolution of $\pm 0.1°C$. To reduce the complexity of the model and the cost of the setup, only the dominant structures of the robot which expand to a relevant amount were equipped with a sensor and considered for thermal correction. For both of the experimentally exploited robots, the structure suggests that the base link, as well as links 1-3, predominantly influence the total thermal drift of the TCP. This presumption was verified experimentally (see section VI-C). The exact locations of the temperature sensors are marked in figure 2.

D. Software Architecture

In order to be able to apply the error compensation robot-independently, the communication with the robot is performed using the Robotic Operating System (ROS). This widely used robotics middleware allows to deploy a variety of well-proven functionalities like collision-aware path planning, trajectory controls, or sensor drivers. Figure 6 illustrates the software architecture that is used for error compensation. In addition to the error correction, the high-level joint state trajectory is optimized using the Python library TOPPRA [41] to ensure smooth accelerations on joint level.

This article has been accepted for inclusion in a future issue of this journal. Content is final as presented, with the exception of pagination.

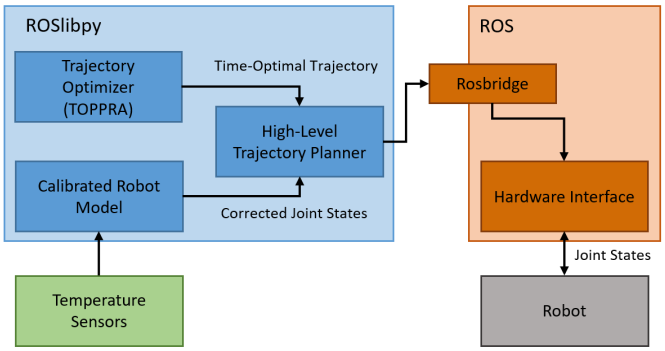

Fig. 6. Robot-independent software architecture for error compensation.

V. Design of Experiments

A. Data Sets

To verify that the proposed modeling approaches are able to compensate for the respective aspects, multiple data sets were recorded comprising different disturbing effects. To facilitate the explanations in the subsequent analysis, the following identifiers are used:

- **UniDir:** 300-400 randomly selected poses were measured, approaching from negative joint rotation direction at steady-state link temperature.
- **MultiDir:** 300-400 randomly selected poses were measured, approaching from random joint rotation direction at steady-state link temperature.
- **ThermTrain:** Thermal training set comprising 300-400 randomly selected poses, approached from random joint rotation direction. A heat-up trajectory is performed repetitively where all motors are thermally excited.
- **ThermVal:** Thermal validation set comprising 300-400 randomly selected poses, approached from random joint rotation direction. A heat-up trajectory is performed repetitively where the motors of joints $1, 2$ and 5 are thermally excited. This data set represents a separate set of randomized sample points, to expose potential effects of overfitting.

These data sets have then been used to identify a subset of the model parameters and validate the results. For the identification process, five cases were distinguished, where (i) only the location of the base and end-effector frame (see nominal pose accuracy described in V-D), (ii) the kinematic model parameters, (iii) the kinematic and backlash parameters, (iv) the kinematic and thermal parameters, and (v) the full model, i.e., kinematic, backlash, and thermal parameters, are identified. This procedure allows to separately test the individual models that have been fused in the proposed work.

B. Measuring Technique

To reduce measurement noise, the median of 240 measurement points (corresponding to 3 seconds of continuous measurement) is taken for each data point. Since the time constant of thermally induced variations of the structure is by magnitudes larger and no other time constraint is present for the calibration, this procedure does not influence the results. Furthermore, to ensure small and reproducible deceleration, the last $0.15\ deg$ of joint revolution is covered within a second. That way, arbitrary misalignment within the dead zone of the joint backlash is reduced to a minimum.

C. Evaluation Metrics

To assess the positioning accuracy, the average of the positioning error defined by

$$\bar{P} = \frac{1}{n}\sum_{j=1}^{n}\left\|\mathbf{p}_j - \mathbf{p}_j^*\right\| \tag{18}$$

was used, where $\|\cdot\|$ describes the Euclidean norm, $\mathbf{p}_j$ denotes the measured end-effector position at pose j, $\mathbf{p}_j^*$ refers to the commanded position and n is the number of measurements taken in the given experiment. Furthermore, the corrected standard deviation given by

$$\sigma_P = \sqrt{\frac{\sum_{j=1}^{n}(P_j - \bar{P})^2}{n-1}} \tag{19}$$

and the maximal positioning error, denoted P_{max}, were evaluated. The use of the most commonly used evaluation metrics simplifies the comparison with literature and allows for an intuitive interpretation.

For the results presented below, all stated errors are statistical means over a large sample size. We therefore chose to faithfully represent the results as they were computed, with a precision that exceeds the expected accuracy of the measuring device (which is $0.1mm$ volumetric accuracy).

D. Nominal Pose Accuracy

This metric allows to benchmark the pose accuracy of the uncalibrated robot. To make sure that no additional errors are introduced by a potential misalignment of the measurement coordinate systems, two homogeneous transformation matrices describing the transformations from the world frame to the robot base $T_{w,b}$ and from the robot end-effector to the tracking target $T_{ee,t}$ are introduced. These transformation matrices can be used to correct the estimated pose of the tracking target and are given by

$$\mathbf{T}_{w,t} = \mathbf{T}_{w,b} \cdot \mathbf{T}_{b,ee}(\mathbf{x}_{nom}, \mathbf{q}) \cdot \mathbf{T}_{ee,t}, \tag{20}$$

where the nominal model parameters $\mathbf{x}_{nom}$ can be found in the datasheets provided by the manufacturer of the robot. This corrected forward kinematics can then be used to identify the parameters of $T_{w,b}$ and $T_{ee,t}$ while holding the robot parameters constant. This can be done using the objective function given in 12 by replacing the estimated pose $\mathbf{p}_{ee}(\mathbf{x}, \mathbf{q}_i)$ with the corrected one $\mathbf{p}_{w,t}(\mathbf{x}, \mathbf{q}_i)$. The described procedure ensures a precise evaluation of the nominal robot model.

VI. Experimental Results

The main goal of the experiments conducted in this work is to validate the novel combined robot model and assess the positioning performance when applying it. However, to establish the significance of the individually studied effects and provide benchmarks for this validation, in the first step

This article has been accepted for inclusion in a future issue of this journal. Content is final as presented, with the exception of pagination.

TABLE III
SUMMARY OF EXPERIMENTAL RESULTS OF THE MULTIDIR DATA SET

Robot	Metric	Nominal model	Kin. calibration	Kin. & backlash	Kin. & thermals	Kin., backlash & thermals
KR-16	$\bar{P}$ $[mm]$	3.33	**0.10**	-	-	-
	σ_P $[mm]$	1.88	**0.06**	-	-	-
	P_{max} $[mm]$	8.45	**0.33**	-	-	-
KR-30	$\bar{P}$ $[mm]$	0.29	**0.09**	-	-	-
	σ_P $[mm]$	0.18	**0.04**	-	-	-
	P_{max} $[mm]$	0.89	**0.24**	-	-	-

TABLE IV
SUMMARY OF EXPERIMENTAL RESULTS OF THE MULTIDIR DATA SET

Robot	Metric	Nominal model	Kin. calibration	Kin. & backlash	Kin. & thermals	Kin., backlash & thermals
KR-16	$\bar{P}$ $[mm]$	3.33	0.13	**0.10**	-	-
	σ_P $[mm]$	1.81	0.06	**0.06**	-	-
	P_{max} $[mm]$	8.47	0.36	**0.30**	-	-
KR-30	$\bar{P}$ $[mm]$	0.31	0.10	**0.08**	-	-
	σ_P $[mm]$	0.20	0.05	**0.04**	-	-
	P_{max} $[mm]$	0.89	0.29	**0.27**	-	-

experiments are presented that use only the kinematic and backlash models. Furthermore, an analysis of the influence of the size and shape of the workspace is conducted to help interpreting the resulting positioning errors and researching the origin of the remaining positioning errors.

A. Kinematic Model

In the first experiment, the pure kinematic calibration is assessed. To this end, the kinematic error compensation is applied to the UniDir data set, and the resulting positioning errors are compared to the nominal positioning accuracy. The attained positioning errors are summarized in table III.

The results show that both the average positioning error and the variability are reduced significantly after applying the kinematic calibration for both robots. For the KR-16, the mean position error reduces by 97% (σ_P by 97%) and for the KR-30 it reduces by 69% (σ_P by 78%).

B. Backlash Model

To determine the performance of the backlash compensation, the MultiDir data set is used. Compared to the previous one, this set includes movements with different joint rotation directions and thus introduces backlash errors. Two versions of the compensation model were applied: the first, as before, compensating for kinematics only; the second compensating for backlash as well. The results of this analysis are given in table IV. A comparison of the errors obtained with just kinematic calibration (column 4) to the respective values of the previous experiment (table III, column 4) reveals the amount of positioning error due to backlash. A significant effect can be observed mainly for the KR-16, with an increase in the mean error of $0.03mm$. After applying the combined kinematic and backlash compensation (table IV, column 5), the respective error is reduced by about the same amount, leading to an accuracy virtually identical to the results obtained on the backlash-free UniDir data set.

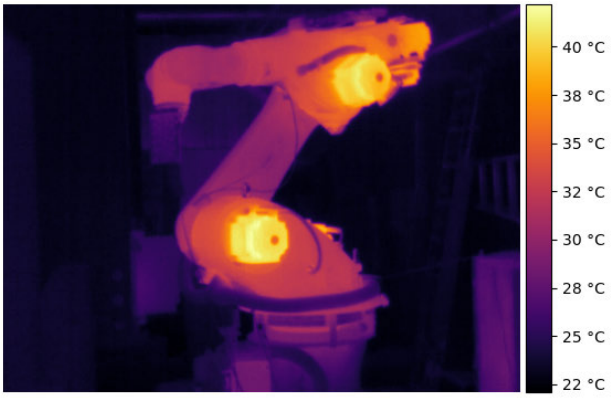

(a) Temperature distribution after ThermTrain.

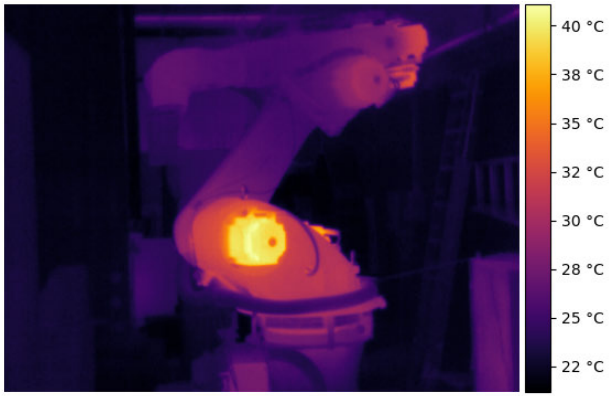

(b) Temperature distribution after ThermVal.

Fig. 7. Temperature distribution of the KUKA KR-30 after different thermal excitations.

C. Thermal Drift Compensation

For the thermal experiments, all model parameters are identified using the ThermTrain data set. The calibrated models are then applied to the ThermVal data set. These sets differ most notably through the pattern of thermal excitation, as outlined in section V-A. Figure 7 shows the temperature distribution over

This article has been accepted for inclusion in a future issue of this journal. Content is final as presented, with the exception of pagination.

TABLE V
SUMMARY OF EXPERIMENTAL RESULTS OF THE THERMVAL DATA SET

Robot	Metric	Nominal model	Kin. calibration	Kin. & backlash	Kin. & thermals	Kin., backlash & thermals
KR-16	$\bar{P}$ $[mm]$	3.35	0.18	0.16	0.12	**0.10**
	σ_P $[mm]$	1.82	0.09	0.09	0.06	**0.06**
	P_{max} $[mm]$	8.41	0.52	0.46	0.32	**0.32**
KR-30	$\bar{P}$ $[mm]$	0.34	0.18	0.16	0.11	**0.09**
	σ_P $[mm]$	0.16	0.08	0.09	0.05	**0.04**
	P_{max} $[mm]$	1.01	0.40	0.44	0.28	**0.28**

TABLE VI
SUMMARY OF EXPERIMENTAL RESULTS OF THE THERMVAL DATA SET

Robot	Metric	Nominal model	Kin. calibration	Kin. & backlash	Kin. & thermals	Kin., backlash & thermals
KR-16	$\bar{P}$ $[mm]$	3.39	0.21	0.20	0.15	**0.13**
	σ_P $[mm]$	1.59	0.08	0.08	0.07	**0.07**
	P_{max} $[mm]$	8.62	0.42	0.38	0.39	**0.35**
KR-30	$\bar{P}$ $[mm]$	0.36	0.20	0.20	0.13	**0.12**
	σ_P $[mm]$	0.19	0.10	0.11	0.06	**0.05**
	P_{max} $[mm]$	1.03	0.56	0.58	0.33	**0.30**

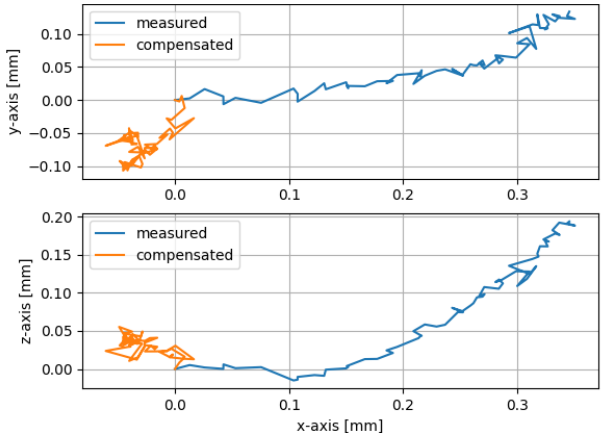

(a) Thermal drift during heat up in ThermTrain.

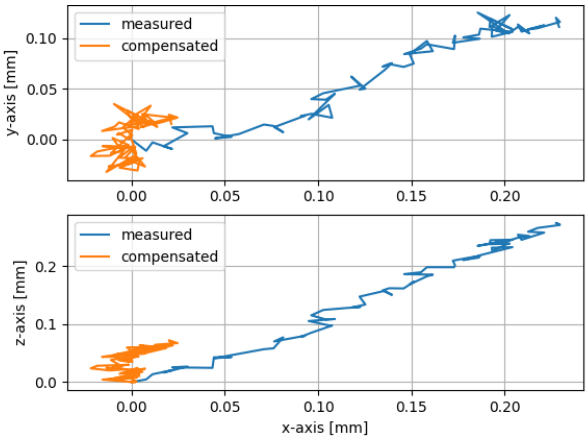

(b) Thermal drift during heat up in ThermVal.

Fig. 8. Thermal drift in xy- and xz-plane at p_{ref} captured with the KUKA KR-30.

the KR-30 captured with the FLIR 50 camera, after executing the substantially different thermal excitation procedures of ThermTrain and ThermVal.

The performance of the thermal expansion model is assessed by measuring the drift of the end-effector positions at a reference position ($p_{ref} = [1.00, 0.37, 0.77]m$, depicted in figure 4) as the robot undergoes the thermal excitation procedures for the ThermTrain and ThermVal data sets. For this experiment, the KR-30 was used, as its bigger structure suggests larger thermal expansion, which is considered more challenging to compensate for. Figure 8 shows the comparison between the uncompensated and compensated thermal drift of the reference pose. The maximal thermal drift could be reduced from $0.38mm$ to $0.10mm$ (or by 74%) for the thermal excitation of the ThermTrain data set, and from $0.38mm$ to $0.10mm$ (or by 70%) for the ThermVal set.

D. Combined Model

All model parameters are again identified on the ThermTrain data set and the trained models are then applied to the ThermVal data set to investigate their ability to compensate for thermal drift on a previously unknown temperature field. The results of the experiments are summarized in tables V and VI.

A comparison of the attained positioning errors after applying the full model calibration to the ThermTrain data set (table V, column 7) with the previous results in section VI-B (table IV, column 5) shows only very small differences, suggesting that the thermal drift has been corrected by the compensation model for this particular excitation pattern.

An assessment of how these results generalize to a different temperature distribution is then provided through the measured accuracy on the ThermVal data set, using the fully compensated model (table VI, column 7). While the positioning errors are somewhat higher in this case, the compensation model still reduces the thermally induced errors by about two-thirds in this experiment. Namely, due to thermal excitation, we observe an increase in the mean error of $0.10mm$ and $0.12mm$ for the KR-16 and KR-30, respectively (comparing column 5 of

This article has been accepted for inclusion in a future issue of this journal. Content is final as presented, with the exception of pagination.

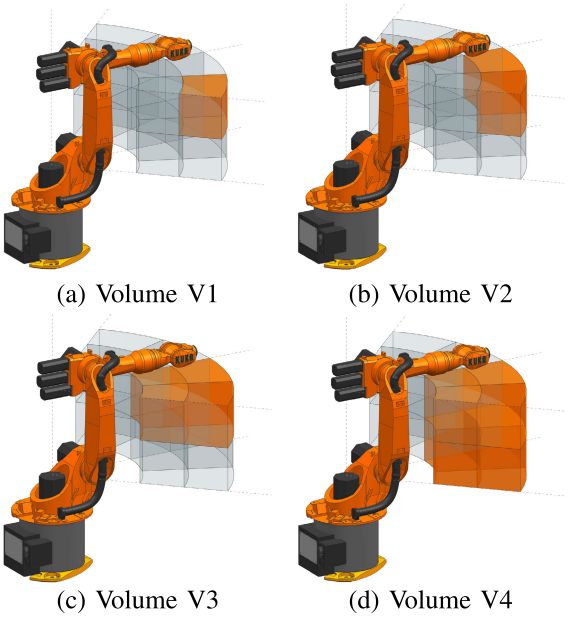

(a) Volume V1 (b) Volume V2

(c) Volume V3 (d) Volume V4

Fig. 9. Illustration of the different subspaces used for analyzing the influence of the size of workspace.

TABLE VII
INFLUENCE OF SIZE OF WORKSPACE ON THE POSITIONING ACCURACY

	V1	V2	V3	V4	full
$\bar{P}$ $[mm]$	0.03	0.05	0.09	0.10	0.10
σ_P $[mm]$	0.02	0.03	0.05	0.06	0.06
P_{max} $[mm]$	0.08	0.16	0.33	0.27	0.30
# of measurements [-]	19	41	85	186	400

table VI, against table IV). The compensation model reduces these to 0.03mm and 0.04mm.

Furthermore, comparing the errors after applying the full model (column 7) to those after kinematic and backlash compensation (column 5) and the ones with kinematic and thermal correction in place (column 6) suggests that the backlash errors are less significant than the ones originating in thermal drift. Namely, the backlash model reduces the average positioning error by 0.01-0.02mm while the thermal compensation reduces it by 0.06-0.08mm.

E. Influence of Size of Workspace

For the subsequent analysis, the nominal workspace is divided into 16 subspaces of equal volume, which are then assembled into four representative workspaces of different size (illustrated in figure 9). To assess the influence of the size and shape of the working envelope on the positioning accuracy, the kinematic and backlash model is trained on the MultiDir data set for each workspace. The KR-16 is used for this analysis because the previous results revealed an inferior positioning accuracy.

The results of the experiments are summarized in table VII. Generally, increasing the workspace negatively impacts the positioning accuracy. The main increase in positioning error was found when adding subspaces in the radial direction (from v2 to v3), almost doubling the positioning error.

VII. DISCUSSION

The following detailed discussion of the above results is structured according to the experiments:

A. Kinematic Model

The comparison between the results after applying the pure kinematic calibration to the UniDir data set (table III) and the nominal robot accuracy show that the mean positioning error can be reduced by 69-97%. This major improvement was expected because of the limited performance of the nominal model. These results of the calibration represent the lower limit of errors attainable with the introduced compensation procedure since none of the subsequently examined disturbances are present in the UniDir data set. To further improve the positioning accuracy, a joint and link compliance correction should be introduced as suggested by *Klimchik & Pashkevich* in [42]. Since the link compliance acts in the same direction as the joint compliance, both effects can be compensated by modeling each joint as a torsion spring.

B. Backlash Model

The experiments show that the backlash effects are significant mainly for the KR-16, increasing the mean positioning error by 0.03mm. The results after applying the backlash compensation for both robots suggest that the method is capable of compensating for the full backlash error, to the extent the measuring accuracy allows to observe.

C. Thermal Drift Compensation

The results of the thermal drift experiments show that the TCP deflection can be reduced by at least 70% for both the ThermTrain and the ThermVal excitations, at the reference position. The experiment suggests that the introduced simplified thermal model successfully captures the main thermal effects and can be applied to a random pose within the workspace. Furthermore, this result reveals that the model adequately generalizes to a different unknown temperature field. The thermal drift compensation could presumably be further improved by using more temperature sensors and increasing the complexity of the mapping function between the measured temperature and the thermal expansion of the links.

D. Combined Model

The experimental data reveals that the thermally induced positioning errors are slightly larger for the KR-30. This suggests that the impact of thermal expansion increases for bigger robotic structures and is therefore harder to correct for. Most importantly, the analysis shows that the thermal positioning errors can be fully compensated on the ThermTrain data set, and are reduced by two-thirds for the ThermVal data set. Although this demonstrates that the model generalizes to an unknown thermal excitation to a large extent, the generalizing property of the thermal model is still limited. To improve the generalization, a more involved thermal model could be adopted and its parameters could be identified using multiple

This article has been accepted for inclusion in a future issue of this journal. Content is final as presented, with the exception of pagination.

data sets with different thermal excitations to reduce the effect of overfitting. At this point, it must be kept in mind, that the thermal excitation of the ThermVal data set substantially differs from the one within the training set. Therefore, the performance on the validation set can be considered a worst-case scenario.

E. Influence of Size of Workspace

Finally, the size and shape of the workspace were investigated regarding its influence on the achieved positioning accuracy. By systematically increasing the workspace, it could be shown that the positional error strongly depends on the radial width of the operation space. This points to the fact that a major part of the remaining positioning error is caused by pose-dependent compliance induced by the weight of the robot structure. The presented analysis shows that these compliance effects can be eliminated by applying the calibration to smaller workspaces. This finding can be exploited to increase the positioning performance by choosing the workspace in a beneficial way according to a given application, or by introducing subspace-dependent robot parameters. Preferably, the subspace division should be performed in configuration space. Note that for the experiment conducted in this work, the number of measured poses increases with the size of the workspace, influencing the statistical confidence of the stated numbers.

The experimental results show that the presented compensation procedure indeed manages to combine various models to compensate for geometric errors, backlash, and thermal drift in a generic way that can be applied to any kind of serial industrial robot. The introduced technique can be used to improve the accuracy within the full workspace and for different thermal excitations or operating conditions. It could be shown that for the given workspace, the mean positioning error, its standard deviation and the maximal positioning error can be significantly reduced for both robots ($\bar{P}^{max} = 0.13mm$, $\sigma_P^{max} = 0.07mm$, $P_{max}^{max} = 0.35mm$).

VIII. Conclusion

The presented work proposes a robot-independent error compensation procedure that is capable of reducing the most dominant disturbances affecting the positional accuracy of articulated robots. The most important findings are:

- The proposed calibration technique successfully combines the compensation of geometrical errors, backlash, and thermal drift.
- All modeled robot properties can be identified simultaneously within a single experiment containing all effects to be identified. This fact ensures optimality of the model parameters and facilitates the application of the compensation method.
- The learned thermal robot characteristics can be applied to different previously unknown temperature fields or operating conditions.
- By assessing the influence of the size of the workspace it could be shown that the compliance caused by the robotic structure itself can be reduced by downsizing the workspace.
- The universal applicability as well as the time-saving and simple calibration method renders the proposed procedure particularly interesting for industrial application.

Acknowledgment

The authors wish to express their appreciation to their esteemed colleague, Dr. Simon Duenser, for his thorough review of the manuscript and the valuable insights he has contributed.

References

[1] B. Mooring, Z. S. Roth, and M. R. Driels, *Fundamentals of Manipulator Calibration*. Hoboken, NJ, USA: Wiley, 1991, pp. 41–44.

[2] Z. Roth, B. Mooring, and B. Ravani, "An overview of robot calibration," *IEEE J. Robot. Autom.*, vol. RA-3, no. 5, pp. 377–385, Oct. 1987.

[3] Z. Li, S. Li, and X. Luo, "An overview of calibration technology of industrial robots," *IEEE/CAA J. Autom. Sinica*, vol. 8, no. 1, pp. 23–36, Jan. 2021.

[4] W. J. Wilson, C. C. Williams Hulls, and G. S. Bell, "Relative end-effector control using Cartesian position based visual servoing," *IEEE Trans. Robot. Autom.*, vol. 12, no. 5, pp. 684–696, Oct. 1996.

[5] F. Janabi-Sharifi, L. Deng, and W. J. Wilson, "Comparison of basic visual servoing methods," *IEEE/ASME Trans. Mechatronics*, vol. 16, no. 5, pp. 967–983, Oct. 2011.

[6] M. Keshmiri and W.-F. Xie, "Visual servoing of a robotic manipulator using an optimized trajectory planning technique," in *Proc. IEEE 27th Can. Conf. Electr. Comput. Eng. (CCECE)*, May 2014, pp. 1–6.

[7] B. Li, W. Zhang, Y. Li, W. Tian, and C. Wang, "Positional accuracy improvement of an industrial robot using feedforward compensation and feedback control," *J. Dyn. Syst., Meas., Control*, vol. 144, no. 7, Jul. 2022, Art. no. 071003.

[8] L. S. Ginani and J. M. S. T. Motta, "Theoretical and practical aspects of robot calibration with experimental verification," *J. Brazilian Soc. Mech. Sci. Eng.*, vol. 33, no. 1, pp. 15–21, Mar. 2011.

[9] R. A. Boby and A. Klimchik, "Combination of geometric and parametric approaches for kinematic identification of an industrial robot," *Robot. Comput.-Integr. Manuf.*, vol. 71, Oct. 2021, Art. no. 102142.

[10] D. Wang, Y. Bai, and J. Zhao, "Robot manipulator calibration using neural network and a camera-based measurement system," *Trans. Inst. Meas. Control*, vol. 34, no. 1, pp. 105–121, Feb. 2012.

[11] X. Chen, Q. Zhang, and Y. Sun, "Evolutionary robot calibration and nonlinear compensation methodology based on GA-DNN and an extra compliance error model," *Math. Problems Eng.*, vol. 2020, pp. 1–15, Jul. 2020.

[12] L.-B. Kong and Y. Yu, "Precision measurement and compensation of kinematic errors for industrial robots using artifact and machine learning," *Adv. Manuf.*, vol. 10, no. 3, pp. 397–410, Sep. 2022.

[13] L. McGarry, J. Butterfield, A. Murphy, and C. Higgins, "Machine learning methods to improve the accuracy of industrial robots," *SAE Int. J. Adv. Current Pract. Mobility*, vol. 5, no. 5, pp. 1900–1918, Mar. 2023, doi: 10.4271/2023-01-1000.

[14] F. C. Park and K. Okamura, "Kinematic calibration and the product of exponentials formula," in *Advances in Robot Kinematics and Computational Geometry*. Dordrecht, The Netherlands: Springer, 1994, pp. 119–128.

[15] L. Wu, R. Crawford, and J. Roberts, "Geometric interpretation of the general POE model for a serial-link robot via conversion into D-H parameterization," in *Proc. Int. Conf. Robot. Autom. (ICRA)*, May 2019, pp. 7360–7366.

[16] S. Hayati and M. Mirmirani, "Improving the absolute positioning accuracy of robot manipulators," *J. Robot. Syst.*, vol. 2, no. 4, pp. 397–413, Dec. 1985.

[17] H. Stone and A. Sanderson, "A prototype arm signature identification system," in *Proc. IEEE Int. Conf. Robot. Autom.*, vol. 4, Mar./Apr. 1987, pp. 175–182.

[18] H. Zhuang, Z. Roth, and F. Hamano, "A complete and parametrically continuous kinematic model for robot manipulators," in *Proc. IEEE Int. Conf. Robot. Autom.*, vol. 1, May 1990, pp. 92–97.

[19] L. Wu, R. Crawford, and J. Roberts, "An analytic approach to converting POE parameters into D–H parameters for serial-link robots," *IEEE Robot. Autom. Lett.*, vol. 2, no. 4, pp. 2174–2179, Oct. 2017.

This article has been accepted for inclusion in a future issue of this journal. Content is final as presented, with the exception of pagination.

[20] A. Müller, "Screw and lie group theory in multibody kinematics: Motion representation and recursive kinematics of tree-topology systems," *Multibody Syst. Dyn.*, vol. 43, no. 1, pp. 37–70, May 2018.
[21] A. Nubiola and I. A. Bonev, "Absolute calibration of an ABB IRB 1600 robot using a laser tracker," *Robot. Comput.-Integr. Manuf.*, vol. 29, no. 1, pp. 236–245, Feb. 2013.
[22] K. Deng, D. Gao, S. Ma, C. Zhao, and Y. Lu, "Elasto-geometrical error and gravity model calibration of an industrial robot using the same optimized configuration set," *Robot. Comput.-Integr. Manuf.*, vol. 83, Oct. 2023, Art. no. 102558.
[23] Y. Cho, H. M. Do, and J. Cheong, "Screw based kinematic calibration method for robot manipulators with joint compliance using circular point analysis," *Robot. Comput.-Integr. Manuf.*, vol. 60, pp. 63–76, Dec. 2019.
[24] R. Luo, W. Gao, and Q. Huang, "POE-based parameter calibration for industrial robots considering joint compliance," in *Proc. 5th Int. Conf. Robot. Autom. Sci. (ICRAS)*, Jun. 2021, pp. 15–22.
[25] Y. Song et al., "Industrial serial robot calibration considering geometric and deformation errors," *Robot. Comput.-Integr. Manuf.*, vol. 76, Aug. 2022, Art. no. 102328.
[26] R. Li and Y. Zhao, "Dynamic error compensation for industrial robot based on thermal effect model," *Meas., J. Int. Meas. Confederation*, vol. 88, pp. 113–120, Jun. 2016.
[27] S. Yin, Y. Guo, Y. Ren, J. Zhu, S. Yang, and S. Ye, "Real-time thermal error compensation method for robotic visual inspection system," *Int. J. Adv. Manuf. Technol.*, vol. 75, nos. 5–8, pp. 933–946, Nov. 2014.
[28] M. Vocetka et al., "Influence of drift on robot repeatability and its compensation," *Appl. Sci.*, vol. 11, no. 22, p. 10813, Nov. 2021.
[29] C. Gong, J. Yuan, and J. Ni, "Nongeometric error identification and compensation for robotic system by inverse calibration," *Int. J. Mach. Tools Manuf.*, vol. 40, no. 14, pp. 2119–2137, Nov. 2000.
[30] A. Le Reun, K. Subrin, A. Dubois, and S. Garnier, "Thermal drift and backlash issues for industrial robots positioning performance," *Robotica*, vol. 40, no. 9, pp. 2933–2952, Sep. 2022.
[31] A. Mueller, "Modern robotics: Mechanics, planning, and control [bookshelf]," *IEEE Control Syst.*, vol. 39, no. 6, pp. 100–102, Dec. 2019.
[32] M. Nordin, J. Galic', and P.-O. Gutman, "New models for backlash and gear play," *Int. J. Adapt. Control Signal Process.*, vol. 11, no. 1, pp. 49–63, Feb. 1997.
[33] B. Wang, J. Liu, and C. Wang, "Measurement and analysis of backlash on harmonic drive," *IOP Conf. Ser., Mater. Sci. Eng.*, vol. 542, no. 1, Jun. 2019, Art. no. 012005.
[34] P. M. Sammons, L. Ma, K. Embry, L. H. Armstrong, D. A. Bristow, and R. G. Landers, "Modeling and compensation of backlash and harmonic drive-induced errors in robotic manipulators," in *Proc. Int. Manuf. Sci. Eng. Conf.*, vol. 2, Jun. 2014, Art. no. V002T02A048.
[35] J. D. James, J. A. Spittle, S. G. R. Brown, and R. W. Evans, "A review of measurement techniques for the thermal expansion coefficient of metals and alloys at elevated temperatures," *Meas. Sci. Technol.*, vol. 12, no. 3, pp. R1–R15, Feb. 2001.
[36] R. He, Y. Zhao, S. Yang, and S. Yang, "Kinematic-parameter identification for serial-robot calibration based on POE formula," *IEEE Trans. Robot.*, vol. 26, no. 3, pp. 411–423, Jun. 2010.
[37] *ISO 9283 Manipulating Industrial Robots—Performance Criteria and Related Test Methods*, Standard ISO/TC 184, International Organization for Standardizations, 1998.
[38] Z. Jiang and M. Huang, "Stable calibrations of six-DOF serial robots by using identification models with equalized singular values," *Robotica*, vol. 39, no. 12, pp. 2131–2152, Dec. 2021.
[39] P. E. Gill, W. Murray, and M. H. Wright, *Practical Optimization*. New York, NY, USA: Academic, 1981, pp. 273–274 and 348–349.
[40] *VXtrack: Dynamic Tracking Measurement Software Module*, CREAFORM, Levis, QC, Canada, 2023.
[41] H. Pham and Q.-C. Pham, "A new approach to time-optimal path parameterization based on reachability analysis," *IEEE Trans. Robot.*, vol. 34, no. 3, pp. 645–659, Jun. 2018.
[42] A. Klimchik and A. Pashkevich, "Serial vs. quasi-serial manipulators: Comparison analysis of elasto-static behaviors," *Mechanism Mach. Theory*, vol. 107, pp. 46–70, Jan. 2017.

Pirmin Sigron received the M.S. degree in mechanical engineering from the Federal Institute of Technology in Zurich (ETH Zürich), Zürich, Switzerland, in 2022. He is currently a Research Engineer with the Advanced Manufacturing Laboratory, ETH Zürich. His current research interests include modeling of thermomechanical systems, robot accuracy enhancement, and industrial automation.

Ivo Aschwanden received the first B.S. degree in electrical engineering from the University of Applied Sciences and Arts Northwestern Switzerland, Brugg-Windisch, Switzerland, in 2008, and the second B.S. degree in mathematics from the Federal Institute of Technology Zurich (ETH Zürich), Zürich, Switzerland, in 2013. He is currently leading the Industrial Automation and Robotics Group, Advanced Manufacturing Laboratory, ETH Zürich. His research interests include reduction of lead time in industrial automation and performance enhancement of stock industrial robots.

Markus Bambach received the Ph.D. and Habilitation degrees from RWTH Aachen University, Aachen, Germany. He is currently a Lead Professor of the Advanced Manufacturing Laboratory, Federal Institute of Technology in Zurich (ETH Zürich), Zürich, Switzerland; and a Professor with the Institute for Novel Manufacturing Technologies, Brandenburg University of Technology, Cottbus, Germany. He was part of the Academic Council of the RWTH Aachen University, from 2008 to 2015. His research interests include hybrid additive manufacturing, high-temperature materials, and integrated computational materials engineering.